# Influence of inertia and aspect ratio on the torsional galloping of single-axis solar trackers

Eva Martínez-García , Eduardo Blanco-Marigorta , Jorge Parrondo Gayo , Antonio Navarro-Manso *

*Energy Department, University of Oviedo, Gijón, Spain*

A B S T R A C T

Single-axis solar trackers are currently one of the cheapest systems for electricity generation. However, they may have to face significant maintenance costs depending on environmental and climatic factors. Weather is believed to provoke approximately half of the damages registered in solar tracker systems, and a large part of them are due to dynamic wind load. Torsional galloping – or, more precisely, flutter with one degree of freedom – is a phenomenon that arises when the wind speed exceeds a certain critical value. It causes the tracker to undergo angular oscillations with increasing amplitude until the structure collapses. The phenomenon is intrinsically linked to geometric and structural parameters, some of which exhibit a wide range of variation in the current market, depending on the configuration and design of the trackers. This article presents an analytical and experimental study on how the onset of torsional galloping is influenced by the inertia of the modules and the aspect ratio of the panel; it also includes the effect of the torque tube stiffness. The analytical study starts from the equation of motion involving the aeroelastic derivatives and the torque equation in differential form. Tests have been conducted on aeroelastic models of the structures of interest. It has been found that the critical reduced velocity of galloping changes with tilt angle, but it is essentially independent of the main structural parameters: torsional stiffness, inertia and aspect ratio. The results are finally presented in a Stability Diagram for the correct and optimal dimensioning of these structures against torsional galloping.

## 1. Introduction

In 2019, the solar tracker market grew by 62% reaching an installed capacity of 23 GWh. Based on those data, technological improvements and energy demand forecasts, that renewable source is expected to grow by 11% per year until 2024 [1].

At present, solar utility-scale installations (see Fig. 1) have one of the lowest levelized costs of electricity production (LCOE) in the renewable energy sector [2]. It is expected that it will soon become the energy source with lowest LCOE of all systems used in the market [3].

This is due to the improvement of the photovoltaic panels and trackers. In the first case, as a result of increased performance and cost reduction due to optimization of the production systems; in the second case, through cost reduction achieved by adjustment of the structural design [4,5].

In this particular, the single-axis photovoltaic solar trackers stand out with an increase in efficiency between 10% and 30% with respect to the fixed panels, depending on the geographical and climatic conditions [6–8].

These structures are composed of a torque-tube oriented north to south, on which the solar panels are mounted. Progressive rotation of that tube (tilt angle) allows the panels to always face the sun direction. The structure is symmetrical with respect to the central driver, which constitutes a fixed point for torsion. The tube is supported by several intermediate pillars that preclude horizontal and vertical motion but allow for free rotation. Fig. 2 shows a structural scheme and details of a common solar tracker.

This structure behaves like a torsion embedded beam, whose torsion constant is defined by the torque-tube; this shaft normally has circular, rectangular or hexagonal cross-sections, with relatively large diameters and small thicknesses to increase rigidity. The inertia, however, is defined by the panels themselves plus the frame that joins them (beams and struts) [9]. The height of the tube above the ground is approximately half the total width of the tracker panel. Fig. 3 shows a simulation image of a tracker by means of Finite Element Method (FEM), which

---

**Nomenclature**

*List of symbols*

| | |
|---|---|
| $A^*_{i,2,3}$ | Aeroelastic derivatives |
| $a$ | Ratio of lengths |
| $b$ | Panel chord |
| $C$ | Limit relationship of $e/D$ for the buckling limit |
| $C_{IO}$ | Inertia coefficient per unit length |
| $Ck$ | Torsional stiffness coefficient |
| $D$ | Diameter of the torque-tube (middle) |
| $D_e$ | External diameter of the torque-tube |
| $D_i$ | Internal diameter of the torque-tube |
| $E$ | Elasticity module |
| $e$ | Thickness of the torque-tube |
| $G$ | Shear module |
| $I$ | Moment of inertia respect to the axis |
| $I_0$ | Moment of inertia respect to the axis per unit length |
| $J$ | Polar moment of inertia |
| $K$ | Reduced frequency |
| $k$ | Tracker torsional stiffness |
| $L$ | Structure characteristic length |
| $M$ | Aerodynamic torque per unit length |
| $m$ | Total mass of the modules |
| $R$ | Radius of the torque tube |
| $T$ | Torque magnitude |
| $t$ | time variable |
| $TI$ | Turbulence intensity |
| $U$ | Wind speed |
| $U^*$ | Reduced velocity |
| $U_{cr}$ | Critical velocity |
| $x$ | Length variable |
| $\theta$ | Angle displacement variable |
| $\rho$ | Air density |
| $\tau_{xy}$ | Cross section shear tension |
| $\upsilon$ | Poisson ratio |
| $\omega_0$ | Natural circular frequency |
| $\xi$ | Damping ratio |



**Fig. 1.** Solar tracker plant.
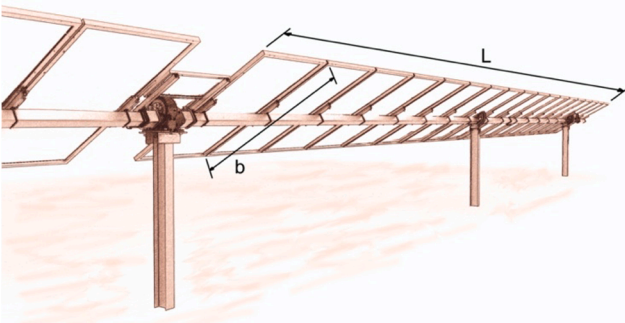


**Fig. 2.** Structural scheme of the solar tracker.

can be used to analyze the influence of the most important structural parameters on the deformation, the natural modes of vibration, etc.

Weather action and climatic events accounts for 49.8% of the causes of structural breakage or collapse of these structures [10]. Among them, one of the main problems they stand is the wind loads. Due to the fact that trackers have evolved to become rather slender structures (for
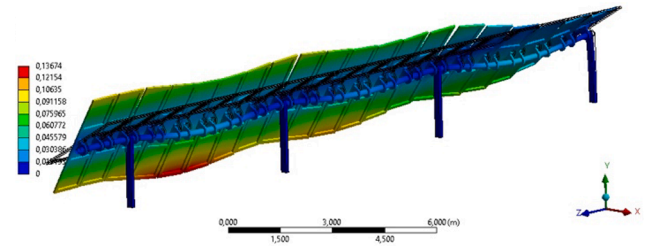


**Fig. 3.** Example of FEM analysis of the first natural mode of vibration.

economic reasons), they are now prone to suffer aeroelastic effects. This implies that the usual static design criteria are not valid when the structure begins to exhibit oscillations, not even if considering a dynamic amplification factor (DAF) [11–14]. Furthermore, international standards do not yet specifically include this type of structure nor the aeroelastic phenomena that may affect them.

There have been numerous studies on the aerodynamic forces in structures such as heliostats and solar panels with a limited aspect ratio, such as [15,16], and also, on the aerodynamic forces in solar arrays, including DAFs, as for example in [17–19].

In particular, one of the most destructive phenomena, which affects many single-axis solar tracker structures, has been identified to be the one degree of freedom flutter (1DOF), commonly called torsional galloping in this industry sector [20–22]. This phenomenon manifests in that, when wind speed exceeds a certain critical value, the tracker begins to vibrate in the first torsional mode of the structure. The amplitude grows rapidly with the wind speed, until the structure collapses due to the breakage of one of its elements.

To date, however, publications on the phenomenon of torsional galloping in single-axis solar trackers are very scarce. Some authors [11] described the phenomenon and explained with some detail the case of initial tilt angle close to $0°$. They also shown some preliminary results of a numerical model validated with an experimental sectional model.

More recently [23], a study on the dynamic forces on these structures has been conducted, by means of a new method that combines aeroelastic measurements in a sectional model with numerical calculations. Although this study was not really focused on instability but on the analysis of buffeting for multi-row trackers, they determined the aeroelastic derivatives to be integrated in their calculation method.

Finally, it has been found that the critical wind speed at which the

instability begins is a function of the tilt angle of the solar tracker [24]. In the stability diagram of Fig. 4 which represents the wind speeds that cause aeroelastic instability for each initial position, the lowest values are found for positive angles close to 20° and a broader range of negative angles, from −15° to −40°. For angles near 0° the critical velocity reaches a somewhat higher value, and for angles higher than 40° or lower than −50° the critical velocity increases rapidly, and the phenomenon even disappears.

However, that set of results has not yet become part of the standards, and there is insufficient data for a reliable design of these structures against aeroelastic effects. As a contribution to fill that gap, an in-depth study is now presented on the critical velocity at which the instability begins over the operating range of angular positions.

This paper first examines the structural characteristics of the single axis solar trackers on the market and describes the dimensionless parameters and aeroelastic variables involved in the phenomenon. This is followed by a description of the experimental procedure used to study the galloping on a series of scale models of trackers with different inertias and aspect ratios. In the next section, the results for each of these two variables are analyzed and the hypotheses used are discussed, as well as the transformation relationships between trackers. Finally, the stability diagram consisting of the determination of the reduced critical speed for each tilt is shown and a study of the optimization of the dimensions to minimize the risk of galloping is made.

## 2. Structural characteristics

Table 1 lists a wide range of standard configurations of solar trackers on the market. It shows the following parameters: the total length *2·L* and width *b* of the tracker-panel, its inertia, the type of photovoltaic modules and the total number *N* of modules mounted on the tracker-panel. The most common modules have dimensions of about 1 × 2 m. Typical module layouts are: 1MIP (1 module in portrait), with a width of approximately 2 m, and 2MIP with a width of approximately 4 m. It is also possible to find 3MIL layouts (3 modules in landscape) and even install 0.5 × 1 m modules in 6MIL layout.

As for the type, the main division between the solar modules that are installed is made in relation to their economic efficiency and their weight: crystalline panels and thin film (Tf). In turn, for the crystalline ones, although they can be divided into monocrystalline and polycrystalline, the parameter that most affects their mass is the mono (1F) or bifacial (2F) configuration. The usual weight of these panels is between 10 and 15 kg/m².

The main structural properties that influence the galloping critical velocity are the stiffness *k*, the inertia *I*, the damping ratio ξ and the geometry configuration. The main geometrical parameter is the aspect ratio, *AR*, although other factors that can affect the phenomenon include the height of the axis above the floor, the separation between panels and the

**Table 1**
Characteristics of commercial trackers.

| Id | Type | Num. modules | b (m) | 2L (m) | I (kg·m²) |
|----|------|--------------|-------|--------|-----------|
| 1 | 1F | 60 | 3.0 | 40 | 704 |
| 2 | 2F | 90 | 4.0 | 45 | 2127 |
| 3 | Tf | 90 | 4.0 | 45 | 1495 |
| 4 | 1F | 90 | 4.3 | 47 | 2274 |
| 5 | 1F | 270 | 3.6 | 54 | 2072 |
| 6 | 1F | 90 | 4.0 | 55 | 2458 |
| 7 | 2F | 120 | 4.0 | 60 | 2836 |
| 8 | Tf | 120 | 4.0 | 60 | 1994 |
| 9 | 1F | 120 | 4.3 | 63 | 3033 |
| 10 | 2F | 90 | 2.0 | 90 | 570 |
| 11 | Tf | 90 | 2.0 | 90 | 401 |
| 12 | 1F | 90 | 2.1 | 94 | 604 |
| 13 | 1F | 240 | 1.8 | 96 | 501 |
| 14 | 1F | 78 | 2.0 | 96 | 570 |
| 15 | 2F | 100 | 2.0 | 100 | 633 |
| 16 | Tf | 100 | 2.0 | 100 | 446 |
| 17 | 1F | 100 | 2.1 | 107 | 651 |
| 18 | 2F | 180 | 2.0 | 180 | 1140 |
| 19 | Tf | 180 | 2.0 | 180 | 802 |
| 20 | 1F | 180 | 2.1 | 189 | 1209 |

torque tube, the dimensions of the struts (depth and width) and the separation between the panels.

The influence of the properties can be analyzed from the following equation describing the torsional movement of the structure per unit length [11]:

$$I_0\ddot{\theta} + 2I_0\xi\omega_0\dot{\theta} + \frac{k}{L}\theta = M \tag{1}$$

where $I_0$ is the torsional inertia per unit length, $\omega_0$ is the natural circular frequency, and θ the angular displacement variable. The first term on the left of the equation corresponds to the inertial forces, the second term includes the effects of damping and the third term is the elastic forces, in this case torsional ones.

The right-hand term *M* is the aerodynamic torque per unit length. To study the beginning of the aeroelastic instability, these moments can be written as a function of the flutter derivatives according to [25]:

$$M = \frac{1}{2}\rho U^2 b^2 \left( K\frac{b}{U}A_2^*\dot{\theta} + K^2 A_3^*\theta \right)\# \tag{2}$$

where *K* is the reduced frequency (inverse of the reduced velocity), *b* a characteristic length (chord), *U* is the wind speed and $A*_i$ are the flutter derivatives or Scanlan coefficients involved in the decoupled two-dimensional torsion. The term with the first derivative of the angle is the aerodynamic damping, and the term that multiplies the angle is the aerodynamic stiffness. The $A*_i$ coefficients are purely aerodynamic and a function only of reduced velocity, i.e., for a given geometric shape of
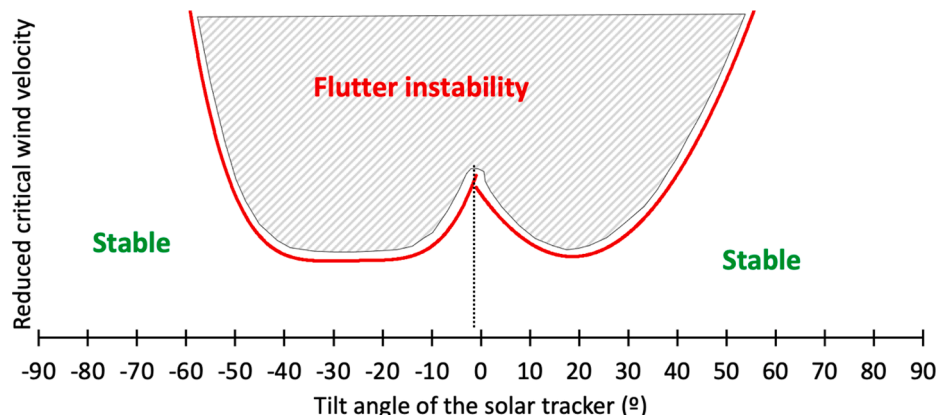


**Fig. 4.** Conceptual Stability Diagram of single-axis solar tracker.

the section, they are independent of the mass, stiffness, and structural damping of the design [26].

Putting together the structural and aerodynamic terms, the resulting differential equation will be unstable if the damping term is negative:

$$\xi - \frac{\rho U b^3 K A_2^*}{2 I_0 \omega_\theta} < 0 \qquad (3)$$

The critical velocity for torsional galloping could be obtained from this equation. In the case of solar trackers each initial angular position implies a different geometrical shape (different $A^*_i$), which means that the critical reduced velocity of galloping varies with the tilt.

As can be seen from Eq. (3), for an instability 1DOF to exist, $A^*_2$ must be positive. It is also observed (and has been proven in the experiments carried out in this research) that when the structural damping is small (<5%), it does not have a significant influence [11]. This is usually the case in steel structures such as solar trackers without external dampers.

Thus, it can be said that instability occurs when $A^*_2$ goes from negative to positive, which occurs at a fixed value of the reduced velocity. Therefore, this implies that the influence of the stiffness, inertia and the aspect ratio in the beginning of the instability occurs only through the reduced velocity.

To study the influence of the structural properties on the critical velocity of galloping, the dimensionless coefficients obtained from the inspectional analysis of Eq. (1) can be used: the damping coefficient $\xi$ itself, and the torsional stiffness $C_k$ and inertia $C_{I0}$ coefficients.

$$C_k = \frac{k}{\frac{1}{2}\rho U^2 L^3} \qquad (4)$$

$$C_{I0} = \frac{I_0}{\frac{1}{2}\rho L^4} \qquad (5)$$

where $U$ is the wind speed and $L$ a characteristic length of the structure.

From Eq. (4), the relationship between the velocities between two similar trackers with different stiffness is:

$$U_2 = U_1 \sqrt{\frac{k_2 L_1^3}{k_1 L_2^3}} \qquad (6)$$

which gives the influence of the stiffness on the critical velocity.

However, the influence of the inertia and the damping ratio cannot be obtained directly from the laws of similarity, since they do not depend on $U$. The same happens regarding the aspect ratio because the geometric similarity is not maintained between models with different $AR$.

## 3. Experimental results

In order to study the influence of the structural characteristics on the galloping critical velocity, aeroelastic tests have been carried out on reduced models of the trackers, with different inertias and aspect ratios. The tests have been performed in the EB40-oWT open wind tunnel, at the Energy Department building of the University of Oviedo. The test section is $0.7 \times 0.7$ m², the maximum speed is about 35 m/s and the nominal power is 30 kW. Other details as well as the nozzle design can be found in [27].

Experiments were conducted under smooth flow conditions. Fig. 5 shows the velocity profile (vertical mid-plane, near the bottom wall), where it can be seen that the boundary layer is about 1 cm. The maximum turbulence intensity is 1.1% in the test section (outside de boundary layer).

Seven scale models were used for this study. The models are composed of up to 3 different materials to correctly reproduce their mechanical and structural characteristics. The shaft is a steel cylinder from 2 to 3 mm of diameter, and it is the responsible of the torsional
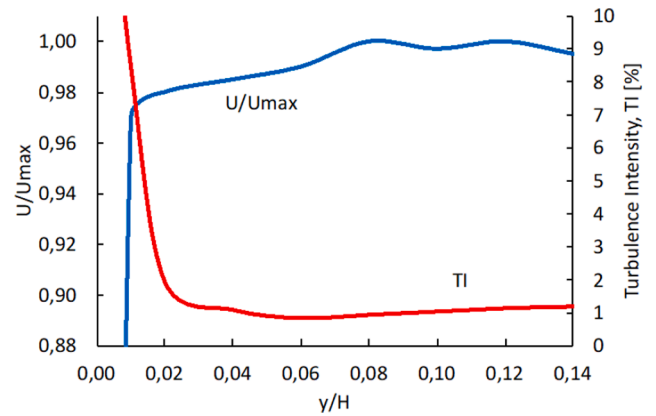


**Fig. 5.** Velocity ratio and turbulence intensity profiles at the outlet of the nozzle of the wind tunnel, near the wall.

stiffness of the model; the solar panel frame has been manufactured in PLA by 3D printing and several types of plastic films have been used for the solar panel in order to adjust the weight and corresponding inertia of these elements. The struts and pillars have also been manufactured in PLA.

The height of the torque-tube above the floor for all models is 1.15 times the semi-chord of the panel. The separation between solar panel and torque-tube is 0.15 times the semi-chord. These dimensions are an average of the values found in the prototypes studied. Table 2 shows the dimensions and structural characteristics of the scale models tested:

The structural damping of all models is less than 1%. Fig. 6 shows all the scale models built on the left, and the detail of assembly of the torque-tube, panels and pillars on the right.

The symmetry of the structure of the solar tracker has allowed to make models of half length $L$, testing only one of the wings of the prototype, from free end to the driver section. This section corresponds to an embedded support (Fig. 7 a), where a force balance has been used to measure the torque. This instrument has 3 load cells (Fig. 7 b) with a range of 2.5 N·m. and accuracy of 0.73%.

The model's tilt positioning system uses a worm gear that allows an angular accuracy of 0.1 degrees (also Fig. 7 b). Tests have been made by changing the tilt angle every 5 degrees, except for positions close to zero, where the increment has been 1 degree. The measurement of the twisted angle (amplitude) at the free end of the tracker is done with a combination of high speed (1000 fps) video and digital photography together with technical drawing software; an accuracy of 0.25 degrees has been achieved.

The air speed in the test section is adjusted with a frequency converter in 0.1 Hz increments which translates into 0.07 m/s. Typical test speeds range from 6 to 15 m/s, with a Reynolds number around $10^5$.

To determine the critical velocity of the instability, the velocity is increased until the model is clearly under galloping (see Fig. 8). Then the velocity is gradually lowered until the oscillation disappears (amplitude less than 0.25 degrees). In this way the critical velocity limit is approached with the tracker in motion, which minimizes the effects of static friction. For the experiments performed with this methodology, it

**Table 2**
Characteristics of the scale models.

| Id | L (m) | b (m) | k (N·m) | I (kg·m²) | $\omega_0$ (Hz) |
|---|---|---|---|---|---|
| 1 | 0.677 | 0.067 | 0.200 | 5.43E$^{-6}$ | 48.0 |
| 2 | 0.677 | 0.100 | 0.200 | 3.65E$^{-5}$ | 18.5 |
| 3 | 0.677 | 0.067 | 0.200 | 7.82E$^{-6}$ | 40.0 |
| 4 | 0.677 | 0.067 | 0.200 | 9.24E$^{-6}$ | 36.8 |
| 5 | 0.677 | 0.067 | 0.202 | 1.14E$^{-5}$ | 33.2 |
| 6 | 0.677 | 0.091 | 0.200 | 2.84E$^{-5}$ | 21.0 |
| 7 | 0.677 | 0.134 | 0.900 | 1.34E$^{-4}$ | 20.0 |

**Fig. 6.** Scale models tested and detail of the assembly.
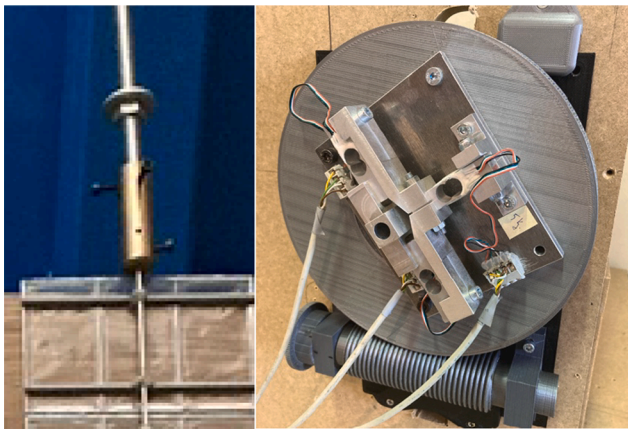


**Fig. 7.** Detail of the anchoring for the driver section (a) and initial tilt positioning system and balance (b).
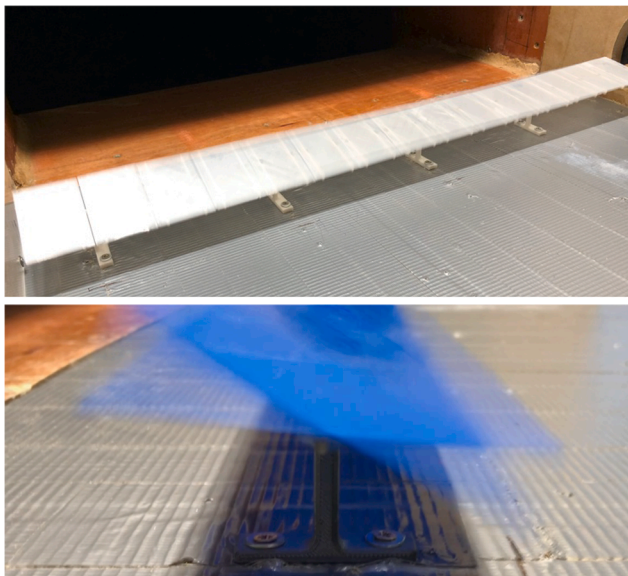


**Fig. 8.** Galloping of the scale model.

has also been found that this velocity is the minimum possible. That is to say, the structure does not fall into galloping for velocities lower than that, even in the face of increased turbulence or other aerodynamic instabilities. This procedure is repeated for each tilt (initial angular position) and the critical velocity values found allow the drawing stability

diagram to be drawn. Fig. 9 shows the corresponding curve for the tracker that has been used as a basis for this study (Id 4 of Table 2):

Fig. 10 shows a power spectra cascade corresponding also to the base case, for −25° tilt, which clearly shows the onset of instability at a reduced velocity of 0.382.

The peak of the beginning of the oscillation occurs at about 33 Hz, while the structure's natural frequency in this case is higher, 36.8 Hz. This is because, unlike Vortex Induced Vibration (VIV), the frequency of the oscillation in flutter is influenced by the aerodynamic damping and stiffness.

Fig. 11 shows one of the models during galloping. The angular deformation can be seen, increasing from the driver to the maximum value of the amplitude at the free end.

In the tests, only one isolated structure was considered, which makes them equivalent to the first-row trackers of the solar plant. The trackers of the second and successive rows would be somewhat protected from the flutter by those of the first row, but being under the influence of the wake, makes them also susceptible to aeroelastic phenomena, and their study requires a specific analysis.

The models have been designed in such a way that they extend across the whole width of the test section and therefore reflect the behavior of a tracker in the middle of the row (the wall in the free end acting as a flow symmetry plane). Several tests have been carried out with the free end in the middle of the flow (simulating an end tracker) and it has been found that the critical velocity is slightly higher, especially for positive tilt angles. As with other structures, the tip effect reduces the aerodynamic forces in that area.

Some checks have also been made by increasing the turbulence in the test section up to 5% using intermediate grids; and it has been found that their effect does not substantially change the critical velocity, only raising it slightly for some tilts.
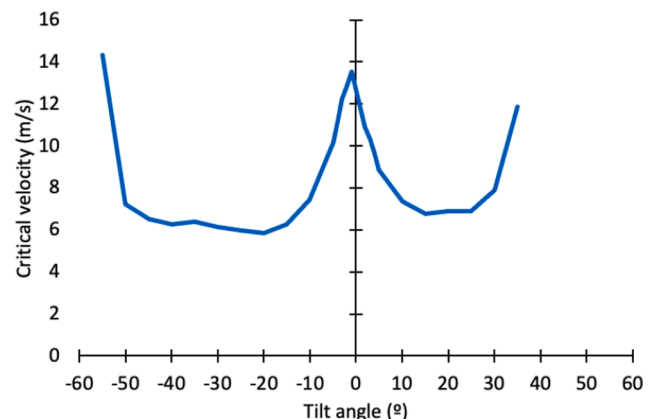


**Fig. 9.** Stability Diagram for a specific tracker.
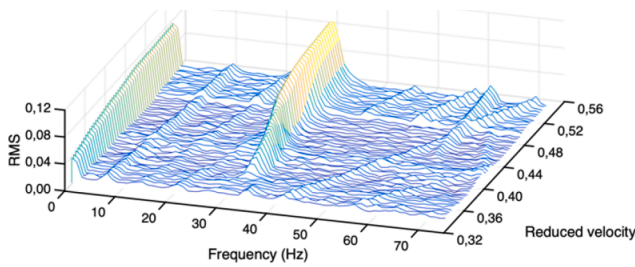
**Fig. 10.** Power spectra Id 4, tilt −25°, RMS torque vs. frequency and reduced velocity.
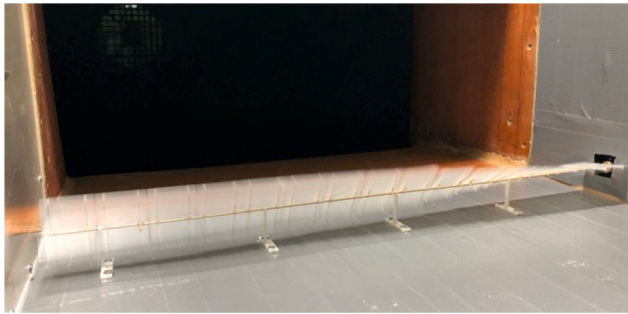


**Fig. 11.** Torsional deflection of the scale model.

Although it has not been specifically studied, the effect of the atmospheric boundary layer on this type of aeroelastic phenomena comes mainly from the reduction of the wind speed at the height of the structure, which implies an increase in the critical velocity [28].

## 4. Analysis of the influence of the inertia and the aspect ratio

For the tracker models and their associated fluid-dynamic phenomena to be fully similar, in addition to the geometric similarity and the non-dimensional stiffness coefficient, the non-dimensional inertia coefficient $C_{I0}$, Eq. (5) must also be maintained. According to this coefficient, the relationship between their inertias must satisfy:

$$I_{02} = I_{01} \frac{L_2^4}{L_1^4} \#$$

(7)

Unlike the ratio obtained for torsional stiffness, Eq. (6), only the dimensions ratio appears in this expression, so it does not allow to calculate the influence of the inertia on the critical velocity. For instance, if two trackers have the same geometrical dimensions then, for them to be similar, they should have the same inertia. If the inertia is different, they are not strictly similar, although the fluid-dynamic phenomenon may be of the same nature.

The typical inertias of the real trackers are shown in Table 1. However, to properly reflect the differences in length, it is more correct to utilize the coefficient of inertia per unit length $C_{I0}$. In the actual trackers studied, this coefficient varies between 0.44 and 1.63 (see Fig. 12). Lower values generally correspond to shorter tracker lengths, and viceversa.

The models that have been tested to determine the influence of the inertia correspond to the Id 1 to 5 of Table 2, which have values of the inertia coefficient between 0.66 and 1.38. Regarding the torsional galloping critical velocity of these models, it has been found that the lower the inertia, the higher the critical velocity.

To be able to compare the different models with each other, the reduced velocity is used. This velocity has been calculated dividing by the width of the panel and the frequency of these structures:
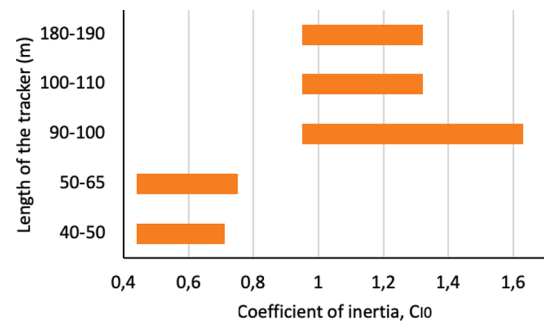


**Fig. 12.** Histogram of the coefficient of inertia $C_{I0}$ as a function of the length of the tracker.

$$U^* = \frac{U}{b\omega_0} = \frac{U}{b} \frac{2}{\pi} \sqrt{\frac{I}{k}} \#$$

(8)

The results nondimensionalized in this way are shown in Fig. 13:

The average value of the differences between the curves (RMS) is less than 5% and is as low as 1% to 2% at the tilt angles where the minimum critical velocities are found. Obviously, the models are not similar because the inertia is different even though they have the same geometry. However, the results indicate that the reduced velocity of galloping is the same for all of them. And not only the starting point but, once the instability starts, the behavior also seems to be closely linked to the reduced velocity, with no direct dependence on inertia.

Fig. 14 shows the amplitude of the torque oscillation at the fixed end (driver) as a function of reduced wind velocity. Several models with different inertia are shown, all for a tilt angle of −25°. In the same Fig. 14 there are also the frequencies (dashed lines) at which the oscillation is produced. They are about 10 to 15% lower than the natural frequency of each tracker. This difference is mainly due to the aerodynamic rigidity. The frequencies remain fairly constant, at least in the galloping range studied, which covers about ±20° of amplitude at the free end of the tracker.

With the aspect ratio something similar to inertia happens: two trackers with different aspect ratios cannot be similar because they do not fulfill the geometrical relations.

To study its influence, the torsion equation for continuous media in partial derivatives with variation over length and time (without the damping term) is used [29]:

$$GJ \frac{\partial^2 \theta(x,t)}{\partial x^2} + M(x,t) = I_0 \frac{\partial^2 \theta(x,t)}{\partial t^2} \#$$

(9)

where $\theta(x,t)$ is the angular displacement of the cross section, $M(x,t)$ is the external torque on the axis per unit length due to the action of the wind, $I_0$ is the moment of inertia per unit length, $G$ is the shear module and $J$ is the polar moment of inertia of the cross section of the axis.

The aspect ratio of single-axis solar trackers is large (>5). In
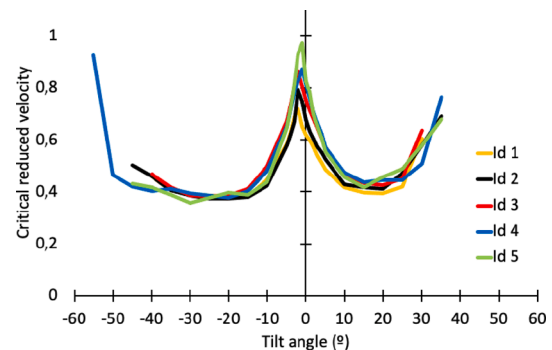


**Fig. 13.** Critical reduced velocities for scale models with different inertia.
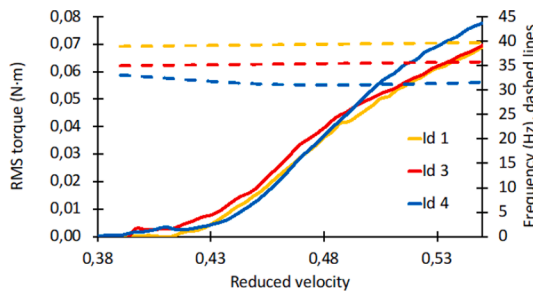
**Fig. 14.** RMS of torque and frequency (dashed lines) vs. reduced critical velocity.

addition, for structures in the middle of the row there is no tip effect. This gives the phenomenon a quasi-bidimensional aspect, despite the twisting along the axis. Then, if a tracker is considered, with the same cross section as another but with a shorter length, and if the angle rotated at the end of both structures is identical, it could be assumed that the phenomenon is the same but compressed. That is, the aerodynamic forces per unit length of tracker are the same in both structures, but in different longitudinal coordinates.

In other words, the hypothesis is based on the assumption that the three-dimensional structure of the fluid-structure interaction can be decomposed into a continuous differential phenomenon and that an integration of the aeroelastic forces over trackers of different lengths can be made basically changing the length variable. This does not mean that three-dimensional phenomena, such as vortex shedding and others, do not exist, but that the integral results of the forces on the driver are equivalent.

Applying the above to Eq. (9), consider two trackers, one of length $L$ and one with a smaller length $L'$; if the variation in length is treated as a change in variable: $(x' = x/a)$, the hypothesis implies that *if* $\theta(x) = \theta'(x')$ then $M(x) = M'(x')$. Performing the change of variable:

$$GJ \frac{1}{a^2} \frac{\partial^2 \theta'(x',t)}{\partial x'^2} + M'(x',t) = I_0 \frac{\partial^2 \theta'(x',t)}{\partial t^2} \# \qquad (10)$$

which would be the same as the equation of the tracker of length $L'$ if its inertia per unit length $I'_0$ was equal to that of the tracker of length $L$ ($I_0$) and its polar module $J'$ was equal to $J/a^2$. In that case, the relation between total inertias would be:

$$I' = \frac{I}{a} \# \qquad (11)$$

And, as the stiffness can be written as a function of the shear module and the polar module:

$$Gk = \frac{GJ}{L} \# \qquad (12)$$

the relationship of stiffness would be:

$$k' = \frac{GJ'}{L'} = \frac{GJ}{La} = \frac{k}{a} \# \qquad (13)$$

Then, if the equations of motion are the same for those two structures, the same air speed will produce the same aerodynamic forces for each differential length, and the same angles at each equivalent position. That is, a total force proportional to the length with the same angle at the end.

In addition, these relationships result in the reduced velocities of these two trackers being the same:

$$U^* = \frac{U}{b} \frac{2}{\pi} \sqrt{\frac{I}{k}} = \frac{U}{b} \frac{2}{\pi} \sqrt{\frac{I'}{k'}} = U'^* \# \qquad (14)$$

To check the validity of this hypothesis, a number of tests have been carried out with experimental models of different aspect ratios. The

aspect ratios of the commercial trackers analyzed vary between 5.5 and 45.6, basically increasing with length (see Fig. 15):

The aspect ratios that have been studied are 5, 7.5 and 10 (Id 4, 6 and 7 in Table 2), which are in the range of the minimum ratios found in the market. No larger ratios have been studied so as not to reduce the scale excessively. However, if the hypothesis made is valid, it is obvious that it will also be valid for higher aspect ratios.

Fig. 16 shows the critical reduced velocities of torsional galloping for the three models as a function of the tilt angle. As was the case for the inertia, the variations between them are very small, on average less than 2.3% and between 0.5% and 1% for the angles of the minimum critical velocities.

Using the similarity relations in the stiffness and those of the aspect ratio, it is possible to deduce the transformation relationships between two trackers.

Consider a tracker with dimensions length $L_1$ and chord $b_1$, with a torsional stiffness $k_1$ and an inertia $I_1$, withstanding a torque $T_1$ at a wind speed $U_1$. Then, a tracker of dimensions length $L_2$ and $b_2$, with a torsional stiffness $k_2$, would have the same behavior as the first one if its inertia $I_2$ is:

$$I_2 = I_1 \frac{L_2}{L_1} \left( \frac{b_2}{b_1} \right)^4 \# \qquad (15)$$

and if the wind speed $U_2$ is:

$$U_2 = U_1 \frac{b_1}{b_2} \sqrt{\frac{k_2}{k_1} \frac{L_1}{L_2}} \# \qquad (16)$$

And it would withstand a torsional force $T_2$:

$$T_2 = T_1 \frac{k_2}{k_1} \# \qquad (17)$$

If the inertias do not meet the ratio of Eq. (15), it can be said, at least, that they have in common the critical reduced velocity, as shown previously.

## 5. Stability diagram and optimal design

According to what has been discussed in the previous sections, it can be concluded that the critical reduced velocity of this type of structures depends on the tilt angle but not on the inertia or aspect ratio. And therefore, the values of this reduced velocity can be represented in the following diagram of stability against galloping. Considering the values of the critical reduced velocity of all models tested, their mean value and standard deviation can be seen in Fig. 17, as a function of tilt:

The minimum average critical velocity value is found for negative tilt angles between −20 degrees and −30 degrees and is approximately 0.37. For these angles the variation is very small (around 1%). The other minimum is found for positive values between 15° and 20°, with a value of 0.4 and a variation of 2%. In the zone of horizontal tilts, the average value of the critical reduced velocity increases up to the range of 0.7 to 1,
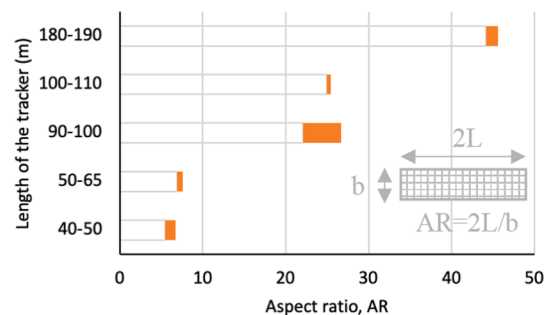


**Fig. 15.** Histogram of the aspect ratio AR as a function of the length of the tracker.
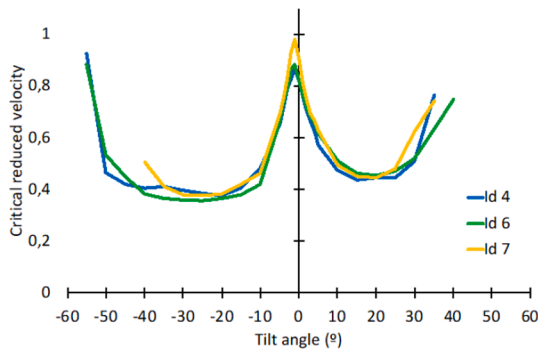
**Fig. 16.** Critical reduced velocities for models with different aspect ratio.
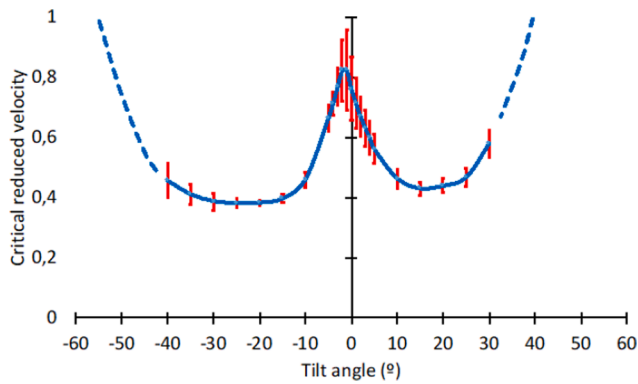


**Fig. 17.** Stability Diagram against torsional galloping: average value and standard deviation of the critical reduced velocity of the trackers tested.

between $-1°$ and $-2°$. For large tilts, both positive and negative, the phenomenon disappears. No galloping has been found above $45°$ or below $-55°$ in any of the models tested. At these extremes the standard deviation also increases, although not as much as in the horizontal angles.

It is believed that the factors that most influence the deviations are the friction of the model shaft with the supports and the gaps in the housings. In the case of angles close to the horizontal, geometric imperfections in the alignment of the leading edge may also be important.

The consistency between the results confirms that the key parameter to avoid torsional galloping is the critical reduced velocity. The relationship with the inertia and the torsional stiffness comes through the natural frequency of the structure.

For the design of a tracker against galloping, the critical velocity can be found with the following equation, taking the minimum values of the critical reduced velocity $U^*_{cr}$ given by Fig. 17:

$$U_{cr} = U^*_{cr} \cdot \frac{b \cdot \pi}{2} \sqrt{\frac{k}{I}} \# \tag{18}$$

This formulation is specific to the torsional galloping or 1 DOF flutter. Other phenomena, such as VIV, have been found in some tests, although only for specific values of speeds and tilts. The amplitude measured has been an order of magnitude lower and disappears as the velocity increases. Another phenomenon that could appear is the flutter of two degrees of freedom (2DOF), if the solar panels were very flexible in their own plane.

The expression of Eq. (18) can be used to optimize the relationship between the length and chord dimensions of the panel. For instance, when designing a tracker with a certain number of modules ($L \cdot b = $ constant), for a fixed weight per square meter, the total inertia of the tracker depends on the width:

$$I = \frac{1}{12} m b^2 \# \tag{19}$$

where $m$ is the total mass of the modules.

However, when substituting in the Eq. (18) of the critical velocity, the result is independent of $b$ (and of $L$):

$$U_{cr} = U^*_{cr} \cdot \frac{\pi}{2} \cdot \sqrt{\frac{12k}{m}} \# \tag{20}$$

Therefore, the only dependence on the inertia is not imposed by the shape but by the mass of the modules: the lower their weight, the higher the galloping critical velocity.

Regarding the torsional stiffness, assuming a thin-walled torque tube, it can be written as:

$$k = \frac{GJ}{L} = \frac{G}{L} \frac{\pi}{32} \left(D_e^4 - D_i^4\right) \approx \frac{G\pi}{8L} D^3 e \# \tag{21}$$

where $D_e$, $D_i$, $D$ are respectively the outer, inner and middle diameters, and $e$ the thickness of the tube.

The ratio of diameter to thickness is ultimately defined by the buckling limit. According to [30] for long thin-walled cylinders, the criterion is:

$$\tau_{xy} = \frac{E}{3\sqrt{2}\left(1 - v^2\right)^{\frac{3}{4}}} \left(\frac{e}{R}\right)^{\frac{3}{2}} \# \tag{22}$$

From where a limit value for the relationship between thickness and diameter $e/D = C$ can be obtained.

The volume of the torque tube will determine its cost (it will be proportional to the weight). The stiffness can be written as a function of that volume and the value imposed by the critical buckling stress:

$$k \approx \frac{G \cdot Vol^2}{\pi 8 C^2 L^3} \# \tag{23}$$

Substituting in Eq. (20):

$$U_{cr} = U^*_{cr} \cdot \frac{1}{L^{\frac{3}{2}}} \cdot \frac{Vol}{C} \cdot \sqrt{\frac{3\pi G}{8m}} \# \tag{24}$$

As it can be seen, the velocity of galloping is finally a function of the length, and the chord does not appear directly. According to this relationship, for a given value of the panel surface ($b \cdot L$), the shorter the length of the structure or the larger the width, the greater the wind speed it can withstand without falling into instability.

Despite the previous analysis, it would be necessary to consider that by increasing the tracker's chord, the wind forces per unit length would increase. This would force an increase in the stiffness of the struts in the plane of the panel, as well as the section and foundation of the pillars. Therefore, the optimal length of the tracker would result from a compromise between these factors.

## 6. Conclusions

In this paper it has been obtained for the first time the Stability Diagram that determines the behavior of a single-axis solar tracker against the phenomenon of torsional galloping. The main contribution of the research is that the galloping critical velocity varies for each tilt, and that the influence of the main structural factors, within the range currently on the market, comes only through the reduced speed.

To this end, the effect of the stiffness in similar models has been examined, and an analytical and experimental study of the influence of the inertia of the modules and the aspect ratio of the panel has been carried out.

To determine the appropriate ranges of these variables, the typical values on existing trackers have been compiled. Currently, these properties are mostly grouped according to the total length of the tracker:

shorter trackers are usually those with lower inertia coefficients and lower aspect ratios, and vice-versa.

Regarding the effect of the inertia, the beginning of the instability has been analyzed from the motion equation and the aeroelastic forces. It has been found that it depends mainly on the sign of the aeroelastic derivative corresponding to the torsional aerodynamic damping. This analysis and the test performed on scale models with different inertia have probed that the critical reduced velocity of torsional galloping does not change with respect to inertia. Likewise, the non-stationary behavior during galloping also seems to be directly related to the reduced velocity.

As for the aspect ratio, it has been assumed that the aerodynamic forces per unit of tracker length are maintained for structures with different aspect ratios, but in different longitudinal coordinates. From this hypothesis, the equations that relate the structural properties between different aspect ratios have been derived analytically. The tests carried out have been focused on the lowest aspect ratio range (the most problematic) and it has been verified that, as with the inertia, the critical reduced velocity of galloping remains constant.

The equations of transformation of structural properties as a function of dimensions and torsional stiffness have also been deduced.

The bulk of the experimental data has been used to plot a Stability Diagram with an average critical velocity line and independent confidence bounds for each tilt angle, as obtained from a standard deviation analysis. This diagram establishes the general criterion of tracker stability against torsional galloping.

Finally, an analysis has been carried out on the optimal design of the tracker. The results show that, for a certain solar capture surface and given dimensions of the torque tube, shorter trackers are more stable with respect to torsional galloping instability, though the wind forces per unit length increase.

## CRediT authorship contribution statement

**Eva Martínez-García:** Software, Methodology, Resources, Data curation, Visualization, Project administration. **Eduardo Blanco-Marigorta:** Conceptualization, Formal analysis. **Jorge Parrondo Gayo:** Validation, Writing - review & editing, Supervision. **Antonio Navarro-Manso:** Investigation, Writing - original draft, Funding acquisition.

## Declaration of Competing Interest

The authors declare that they have no known competing financial interests or personal relationships that could have appeared to influence the work reported in this paper.

## References

[1] Wesoff E. Solar Trackers in Wind and the Terror of Torsional Gallooping. PV Magazine USA; 2020. January 17th. https://pv-magazine-usa.com/2020/01/17/dan-shugar-nextracker-ceo-on-solar-trackers-in-wind-and-the-terror-of-torsional-galloping/.

[2] Lazard. Lazard's Levelized Cost of Energy Analysis – Version 12.0. Lazard, New York, USA; 2018. https://www.lazard.com/media/450784/lazards-levelized-cost-of-energy-version-120-vfinal.pdf.

[3] Energy Information Administration. Levelized Costs and Levelized Avoided Cost of New generation Resources in the Annual Energy Outlook. U.S. Energy International Agency; 2021. https://www.eia.gov/outlooks/aeo/pdf/electricity_generation.pdf.

[4] Talavera DL, Muñoz-Cerón E, Ferrer-Rodríguez JP, Pérez-Higueras PJ. Assessment of cost-competitiveness and profitability of fixed and tracking photovoltaic systems: the case of five specific sites. Renew Energy 2019;134:902–13. https://doi.org/10.1016/j.renene.2018.11.091.

[5] Masson G, Kaizuka I. Trends 2019 in Photovoltaic Applications. (IEA) International Energy Agency; 2019. https://iea-pvps.org/wp-content/uploads/2020/02/5319-iea-pvps-report-2019-08-lr.pdf.

[6] Bahrami A, Onyeka Okoye C, Atikol U. Technical and economic assessment of fixed, single and dual-axis tracking PV panels in low latitude countries. Renew Energy 2017;113:563–79. https://doi.org/10.1016/j.renene.2017.05.095.

[7] Koussa M, Cheknane A, Hadji S, Haddadi M, Noureddine S. Measured and modelled improvement in solar energy yield from flat plate photovoltaic systems utilizing different tracking systems and under a range of environmental conditions. Appl Energy 2011;88:1756–71. https://doi.org/10.1016/j.apenergy.2010.12.002.

[8] Lave M, Kleissl J. Optimum fixed orientations and benefits of tracking for capturing solar radiation in the continental. Renew Energy 2011;36:1145–52. https://doi.org/10.1016/j.renene.2010.07.032.

[9] Galuppi L, Royer-Carfagni G. Enhanced Effective Thickness for laminated glass beams and plates under torsion. Eng Struct 2020;206:110077. https://doi.org/10.1016/j.engstruct.2019.110077.

[10] Pickerel K. How the Solar Industry is Responding to the Increasing Intensity of Natural Disasters. Solar Power World (SPW) 2018, January 29th. https://www.solarpowerworldonline.com/2018/01/solar-industry-responding-increasing-intensity-natural-disasters/.

[11] Rohr C, Bourke PA, Banks D. Torsional instability of single-axis solar tracking systems. In: Proc. 14th Int. Conf. Wind. Eng. 2015, Porto Alegre Brazil, June.

[12] Willuhn M. Tracking in the wind. PV Magazine Australia 2019, September 7th. https://www.pv-magazine-australia.com/2019/09/07/long-read-pt-1-tracking-in-the-wind/.

[13] Davenport AG. The buffeting of large superficial structures by atmospheric Turbulence. Ann N Y Acad Sci 1964;116:135–59. https://doi.org/10.1111/j.1749-6632.1964.tb33943.x.

[14] Jia J. Wind and structural modelling for an accurate fatigue life assessment of tubular structures. Eng Struct 2011;33(2):477–91. https://doi.org/10.1016/j.engstruct.2010.11.004.

[15] Pfahl A, Buselmeier M, Zaschke M. Wind loads on heliostats and photovoltaic trackers of various aspect ratios. Sol Energy 2011;85(9):2185–201. https://doi.org/10.1016/j.solener.2011.06.006.

[16] Stathopoulos T, Zisis I, Xypnitou E. Local and overall wind pressure and force coefficients for solar panels. J Wind Eng Ind Aerodyn 2014;125:195–206. https://doi.org/10.1016/j.jweia.2013.12.007.

[17] Miller RD, Zimmerman DK. Wind Loads on Flat Plate Photovoltaic Array Fields. Seattle, Washington: Boeing Engineering and Construction Company; 1981.

[18] Kopp GA, Farquhar S, Morrison MJ. Aerodynamic mechanisms for wind loads on tilted, roof-mounted solar arrays. J Wind Eng Ind Aerodyn 2012;111:40–52. https://doi.org/10.1016/j.jweia.2012.08.004.

[19] Strobel K, Banks D. Effects of vortex shedding in arrays of long inclined flat plates and ramifications for ground-mounted photovoltaic arrays. J Wind Eng Ind Aerodyn 2014;133:146–9. https://doi.org/10.1016/j.jweia.2014.06.013.

[20] Simiu E. Scanlan RH Wind Effects on Structures: Fundamentals and applications to design. 3th ed. New York: John Wiley & Sons, Ltd.; 1996.

[21] Blevins RD. Flow-Induced Vibration. 2nd ed. New York: Van Nostrand Reinhold Co.; 1990.

[22] Seo D, Caracoglia L. Estimation of torsional-flutter probability in flexible bridges considering randomness in flutter derivatives. Eng Struct 2011;33(8):2284–96. https://doi.org/10.1016/j.engstruct.2011.03.016.

[23] Taylor ZJ, Browne MTL. Hybrid pressure integration and buffeting analysis for multi-row wind loading in an array of single-axis trackers. J Wind Eng Ind Aerodyn 2020;197:104056. https://doi.org/10.1016/j.jweia.2019.104056.

[24] Martínez-García E, Blanco-Marigorta E, Parrondo J, Navarro-Manso A. Experimental determination of the resistance of a single-axis solar tracker to torsional galloping. Struct Eng Mech 2021;78:519–28. https://doi.org/10.12989/sem.2021.78.5.519.

[25] Scanlan RH, Tomko JJ. Airfoil and bridge deck flutter derivatives. J Eng Mech Div 1971;ASCE 97:1717–37.

[26] Wardlaw RL. Flutter and Torsional Instability. In: Sockel H, editor. Wind-Excited Vibrations of Structures. Vienna: Springer; 1994. p. 335. https://doi.org/10.1007/978-3-7091-2708-7_6.

[27] Rodríguez M, Fernández JM, Galdo M, Blanco-Marigorta E, Santolaria C. Novel design and experimental validation of a contraction nozzle for aerodynamic measurements in a subsonic wind tunnel. J Wind Eng Ind Aerodyn 2013;118(3):5–43. https://doi.org/10.1016/j.jweia.2013.04.008.

[28] Fan X, Wang Z, Chen X, Wang Y, Tan W. Experimental investigation on flow-induced vibration of flexible multi cylinders in atmospheric boundary layer. Int J Mech Sci 2020;183:105815. https://doi.org/10.1016/j.ijmecsci.2020.105815.

[29] Rao SS. Vibration of Continuous Systems. New York: Wiley; 2007.

[30] Timoshenko S, Gere JM. Theory of elastic stability. New York: Mc-Graw Hill; 1963.